# Title: Increasing Large Wildfires over the Western United States Linked to Diminishing Sea Ice in the Arctic

**Authors:** Yufei Zou[1*†], Philip J. Rasch[1], Hailong Wang[1*], Zuowei Xie[2] & Rudong Zhang[1]

[1]Atmospheric Sciences and Global Change Division, Pacific Northwest National Laboratory, Richland, WA 99354, USA.

[2]International Center for Climate and Environment Sciences, Institute of Atmospheric Physics, Chinese Academy of Sciences, Beijing, 100029, China.

*Email: yufei.zou@pnnl.gov; hailong.wang@pnnl.gov

[†]Now at: Our Kettle, Inc., Kensington, CA 94707, USA.

**Supplementary Information:**

**Supplementary Discussion:**

**Robust teleconnection in different fire weather and reanalysis datasets**. There are multiple fire weather indices (e.g., FFWI[1]; FWI[2]) derived from different reanalysis datasets available for analyzing the teleconnection relationship between Arctic sea-ice loss and regional fire weather changes. We choose to use FFWI rather than FWI in the main text to keep consistency between reanalysis-based and model-based analyses because FFWI does not require high-frequency hourly meteorological input data that are not available from most modeling outputs for its calculation. Since FFWI is based on surface air temperature, 2-m relative humidity, and surface wind speed without precipitation, we used both FFWI and precipitation (e.g., Fig. 4 in the main text; Supplementary Figs. 3/8) to get a more comprehensive view of surface fire weather conditions. Here we also use two FWI datasets[3,4] derived from different reanalysis data (i.e., ERA5[5]; MERRA-2[6]) to cross-validate the identified teleconnection between the Arctic sea ice and regional fire weather changes as described by ERA5-based FFWI in the main text.

The FWI datasets used for cross-validation purpose are derived from the ERA5 reanalysis data (*T*, RH, precipitation, and wind speed) by Vitolo et al.[3] and the MERRA-2 reanalysis data (T, RH, wind speed, snow depth, and bias-corrected precipitation) in the Global Fire WEather Database[4] (GFWED; https://data.giss.nasa.gov/impacts/gfwed/), respectively. We first calculate the correlations between each pair of the three fire weather index datasets (i.e., ERA5-based FFWI; ERA5-based FWI; MERRA-2-based FWI) as well as their correlations with the HadISST-based SIC time series (Supplementary Table 1). The correlation coefficients among three pairs of the fire weather indices range from 0.71 (between ERA5-based FFWI and MERRA-2-based FWI) to 0.95 (between ERA5-based FWI and MERRA-2-based FWI), with all correlations statistically significant at the 0.001 level. Moreover, the time series of all three fire

weather index data show statistically significant correlations with the SIC time series with the lowest correlation between MERRA-2-based FWI and SIC (r=-0.37; *p*-value=0.02) and the highest correlation between ERA5-based FFWI and SIC (r=-0.68; *p*-value<0.001).

We further re-examine the changes in spatial distributions of regional fire weather as described by the MERRA-2-based FWI data between the SIC- and SIC+ years like what we show by Fig. 1 in the main text. We believe this is a conservative evaluation because of the lowest correlation (but still statistically significant at the 0.05 level) between MERRA-2-based FWI and SIC. As shown by the spatial pattern in Supplementary Fig. 2a, most of the western U.S., especially the Southwestern U.S., also show largely increased FWI values during the SIC- years than the SIC+ years. This is generally consistent with the result shown by the ERA5-based FFWI data in Fig. 1a, albeit the regions with statistically significant fire weather changes expand northward in the ERA5-based FFWI result. Similarly, the months showing significant regional fire weather changes are fewer as suggested by MERRA-2-based FWI (Supplementary Fig. 2c) than that by ERA5-based FFWI, but both data agree that more fire-favorable weather with elevated fire weather indices would occur in autumn and early winter following sea-ice loss in preceding summer. All these results of consistent spatial and temporal changes in regional fire weather confirm a robust linkage between decreasing Arctic sea ice and worsening regional fire weather as described by different fire weather indices (FFWI and FWI) derived from two reanalysis datasets (ERA5 and MERRA-2).

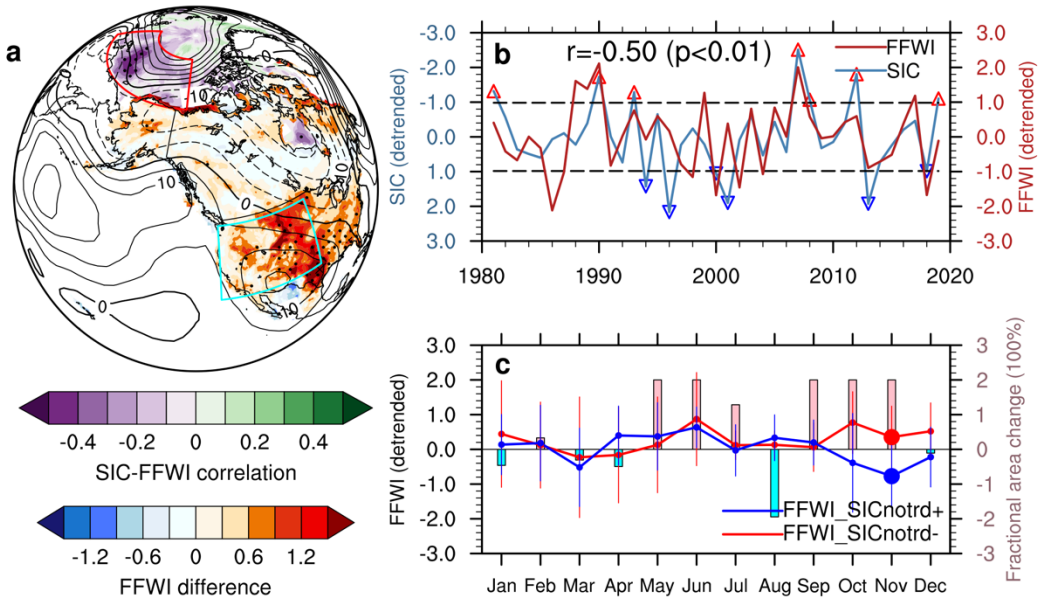


**Supplementary Fig. 1. Observation- and ERA5 reanalysis-based Arctic sea ice and regional fire teleconnection after removing the long-term trends. a**, spatial distributions of the correlation (shading in the Arctic denoted by the purple-green color bar) between seasonal average detrended Arctic sea-ice concentrations in summer and autumn (July to October) and seasonal and regional average detrended FFWI over the western U.S. in the following autumn and early winter (September to December), and the difference of seasonal average detrended FFWI (shading in North America denoted by the blue-red color bar) between years with minimum (SICnotrd-: red up-pointing triangles in **b**) and maximum (SICnotrd+: blue down-pointing triangles in **b**) detrended Arctic SIC. The difference of seasonal (September to December) average detrended geopotential height at 500 hPa between the SICnotrd- and SICnotrd+ years is also shown (contours with negative values in dashed lines; unit: m). Stipples in **a** mark regions that are significantly different from 0 at the 0.05 significance level of two-sided t-tests. **b**, time series of regional and seasonal average detrended SIC (seasonal mean from July to October; first normalized by its 1981-2010 climatological mean and standard deviation

and then detrended; note its scale on the left Y-axis is inverted to directly compare temporal variations of both time series), detrended FFWI (seasonal mean from September to December), and their correlation. The region definitions for the Pacific sector of the Arctic and the western U.S. are outlined by the red and cyan boxes in **a**, respectively. The horizontal dashed lines denote the ±1 standard deviations of normalized and detrended SIC as thresholds for selecting the SICnotrd+/- years. **c**, the composite of monthly detrended FFWI (solid lines with dots and error bars) and fractional detrended burned area change of large wildfires (vertical bars) over the western U.S. Error bars in **c** denote ±1 standard deviations of monthly detrended FFWI in each group. The larger dot for monthly FFWI in **c** denotes the 0.05 significance level of two-sided t-tests for monthly FFWI differences between years with minimum (FFWI_SICnotrd-) and maximum (FFWI_SICnotrd+) detrended Arctic SIC.

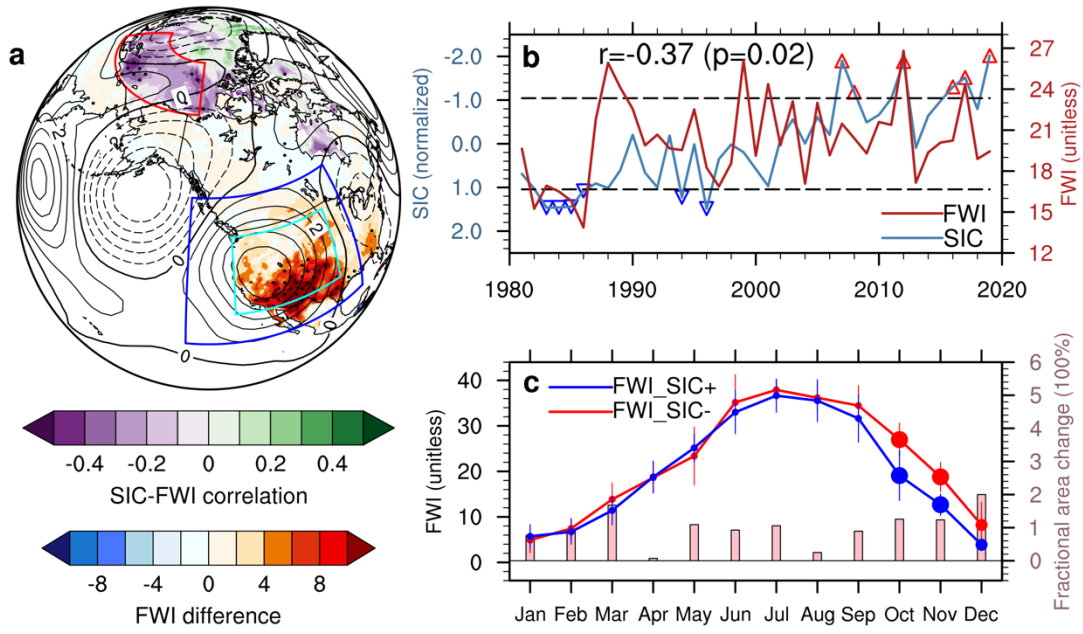


**Supplementary Fig. 2. Observation- and MERRA-2 reanalysis-based Arctic sea ice and regional fire teleconnection. a**, spatial distributions of the correlation (shading in the Arctic denoted by the purple-green color bar) between seasonal average Arctic sea-ice concentrations in summer and autumn (July to October) and seasonal and regional average FWI over the western U.S. in the following autumn and early winter (September to December), and the difference of seasonal average FWI (shading in North America denoted by the blue-red color bar) between years with minimum (red up-pointing triangles in **b**) and maximum (blue down-pointing triangles in **b**) Arctic SIC. The regression of geopotential height anomalies at 500 hPa onto the seasonal and regional average FFWI is also shown (contours with negative values in dashed lines; unit: m). Stipples in **a** mark regions that are significantly different from 0 at the 0.05 significance level of two-sided t-tests. **b**, time series of seasonal and regional average SIC (seasonal mean from July to October; normalized by its 1981-2010 climatological mean and standard deviation; note its scale on the left Y-axis is inverted to directly compare temporal variations of both time series) and FWI (seasonal mean from September to December) and their

correlation. The region definitions for the Pacific sector of the Arctic, the western U.S., and the Z500i projection region are outlined by the red, cyan, and blue boxes, respectively, in **a**. **c**, the composite of monthly FWI (solid lines with dots and error bars) and fractional burned area change of large wildfires (vertical bars) over the western U.S. Error bars in **c** denote ±1 standard deviations of monthly FWI in each group. Dot sizes for monthly FWI in **c** denote the 0.05 (large), 0.1 (medium), and non-significant (small) significance levels of two-sided t-tests for monthly FWI differences between years with minimum (FWI_SIC-) and maximum (FWI_SIC+) Arctic SIC, respectively.

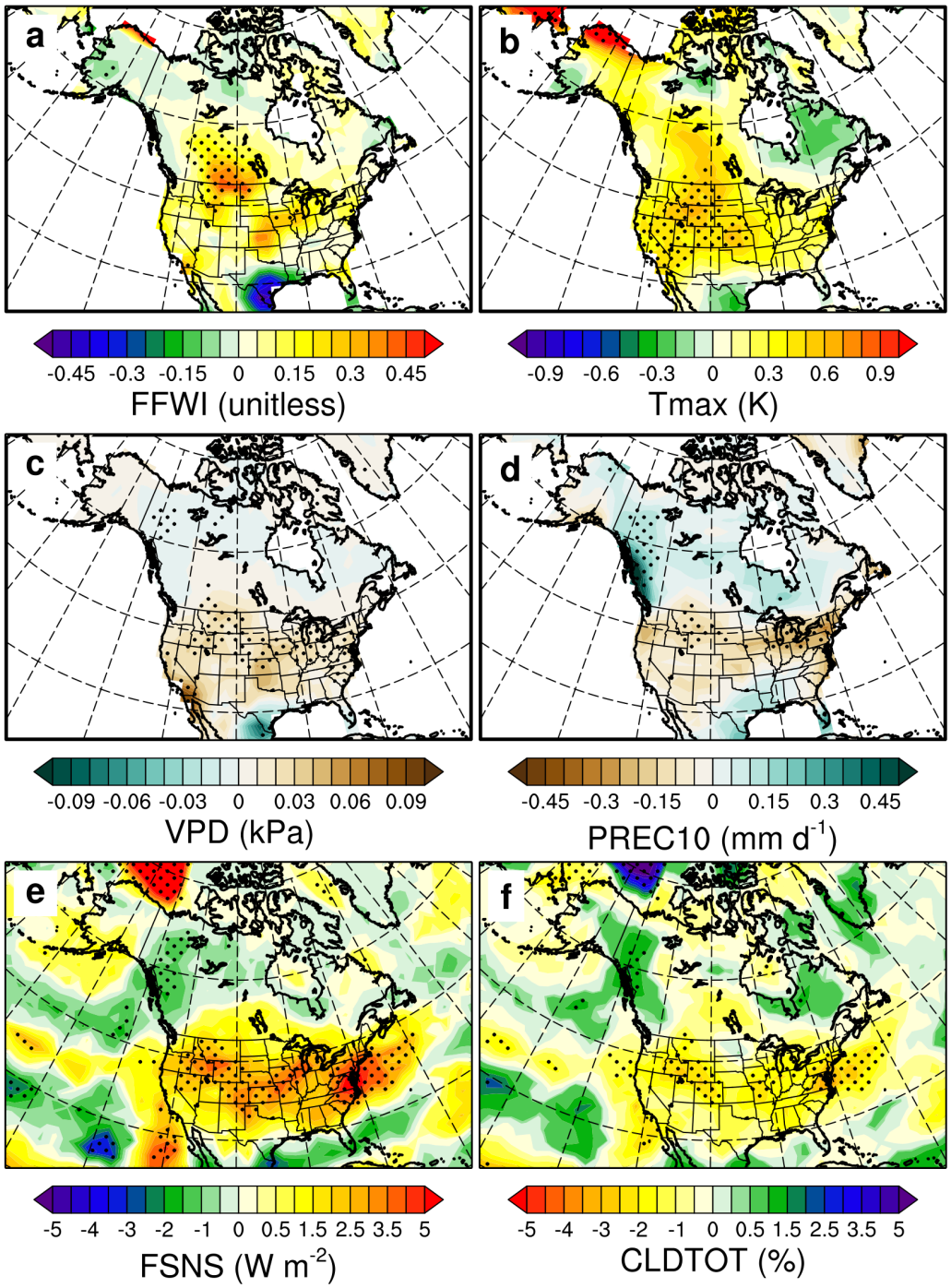


**Supplementary Fig. 3. Fire-related weather responses in the CESM-RESFire experiments.** **a**, the difference of seasonal average (September to December) FFWI between the SICexp- and SICexp+ sensitivity experiments. **b**, as in **a**, but for the difference of seasonal average daily maximum of 2-m temperature (Tmax). **c**, as in **a**, but for the difference of seasonal average

surface vapor pressure deficit (VPD). **d**, as in **a**, but for the difference of seasonal average 10-day running mean of total precipitation (PREC10). **e**, as in **a**, but for the difference of seasonal average net solar flux at surface (FSNS; positive for the downward direction). **f**, as in **a**, but for the difference of seasonal average vertically integrated total cloud fraction (CLDTOT). Stipples in **a-f** show regions that are significantly different from 0 at the 0.1 significance level of a two-sided t-test.

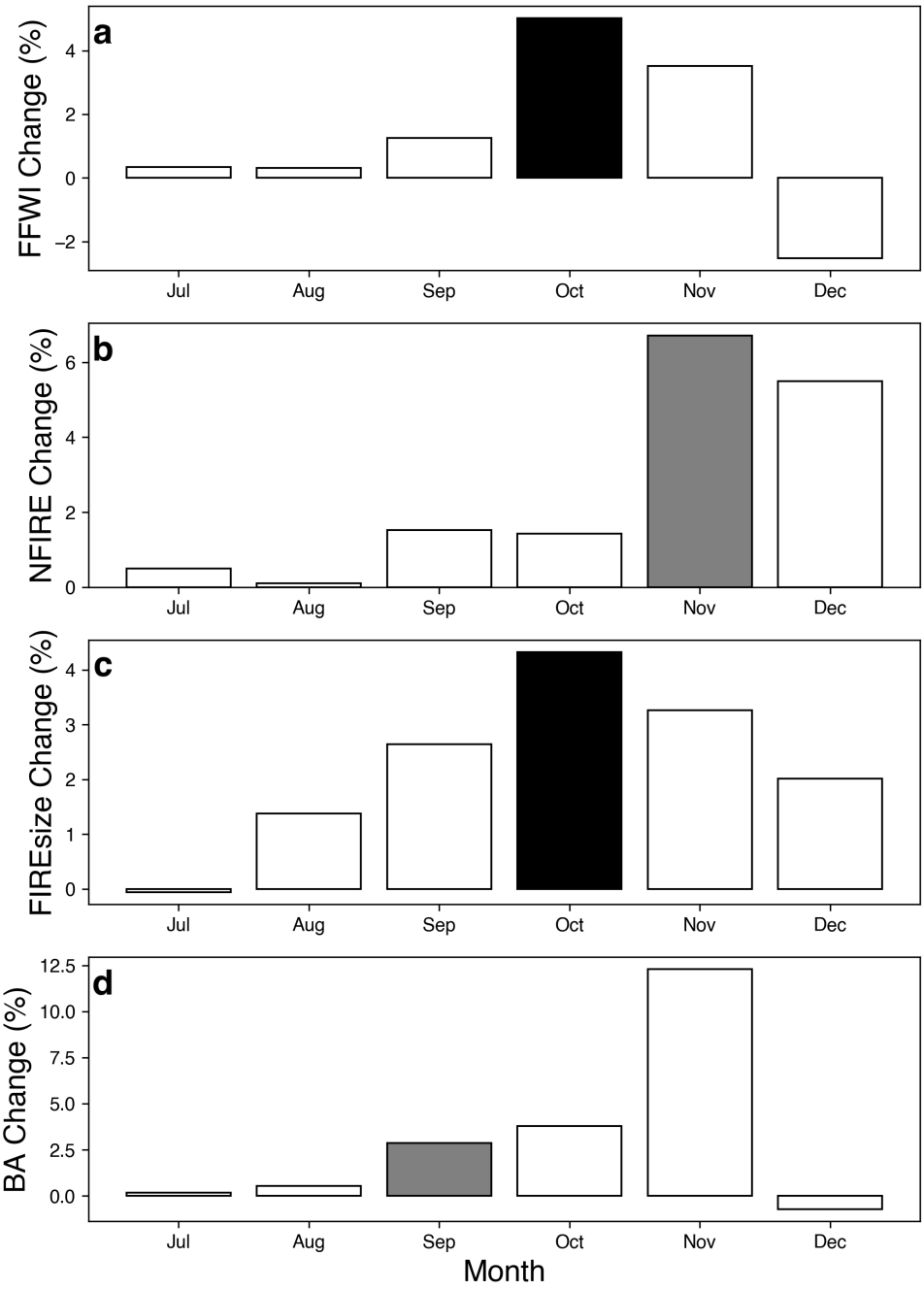


**Supplementary Fig. 4. Fractional changes of monthly fire weather and fire variables in the CESM-RESFire experiments. a**, fractional Changes of regional average FFWI over the western U.S. between the SICexp- and SICexp+ sensitivity experiments. **b**, as in **a**, but for fractional changes of regional total fire counts. **c**, as in **a**, but for fractional changes of regional average fire

123 sizes. **d**, as in **a**, but for fractional changes of regional total burned area. Shadings in **a-d** show
124 fractional changes that are significantly different from 0 at the 0.05 (dark) and 0.1 (grey)
125 significance levels of a two-sided t-test.

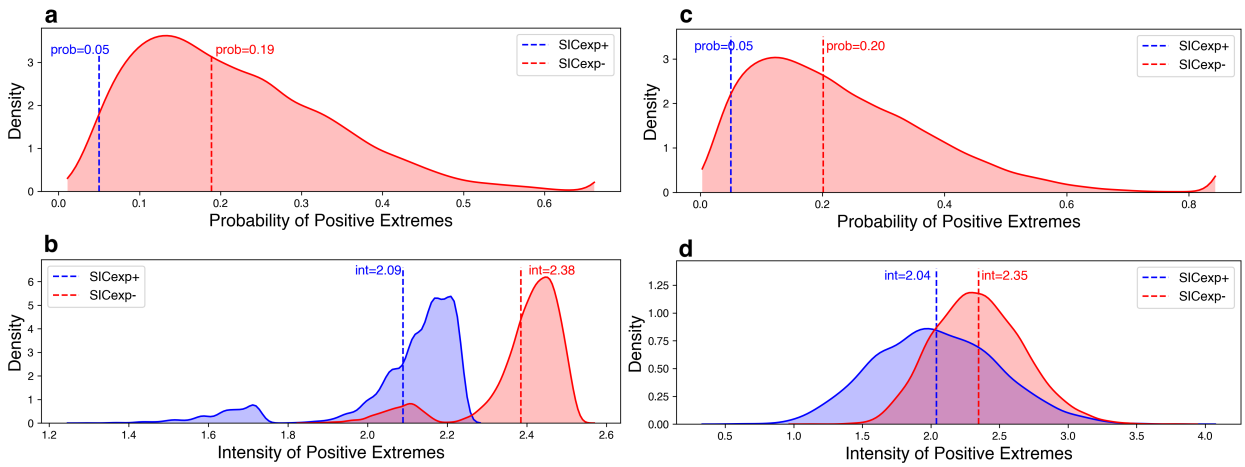


126

127 **Supplementary Fig. 5. Probability and intensity changes of extreme burning years in the**
128 **CESM-RESFire experiments. a**, the statistical distribution for occurrence probability estimates
129 of extreme burning years in the SICexp- and SICexp+ climate sensitivity experiments based on
130 the bootstrap resampling method without replacement (see Methods). The vertical dashed lines
131 denote ensemble mean probabilities for the SICexp- (red) and SICexp+ (blue) experiments. **b**, as
132 in **a**, but for intensity estimates of extreme burning years without replacement in the bootstrap
133 estimation. The vertical dashed lines denote ensemble mean intensity for the SICexp- (red) and
134 SICexp+ (blue) experiments. **c-d**, as in **a-b**, but for the probability and intensity estimates of
135 extreme burning years with replacement in the bootstrap estimation.

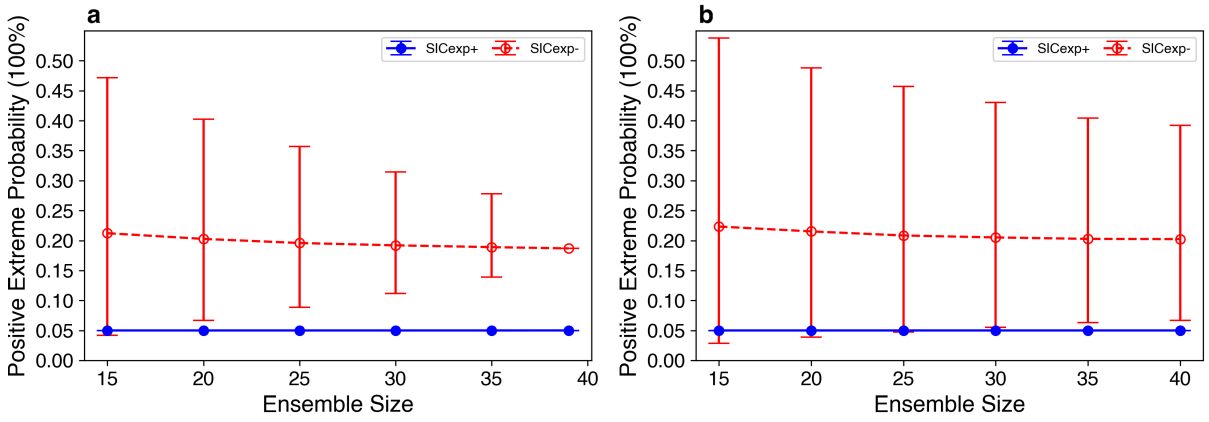


**Supplementary Fig. 6. The relationship between the occurrence probability estimates of extreme burning years and ensemble sizes of the CESM-RESFire experiments. a**, the probability estimates of extreme burning years based on different sizes of ensemble members in the SICexp- and SICexp+ experiments without replacement in the bootstrap method (see Methods). Note the probabilities of extreme burning years in SICexp+ are always 5% by definition. **b**, as in **a**, but for the probability estimates of extreme burning years with replacement in the bootstrap method. The circles in **a-b** denote the ensemble means of the probability estimates, and the lower and upper whiskers denote the 95% (from 2.5% to 97.5%) inter-percentile ranges of the probability estimates.

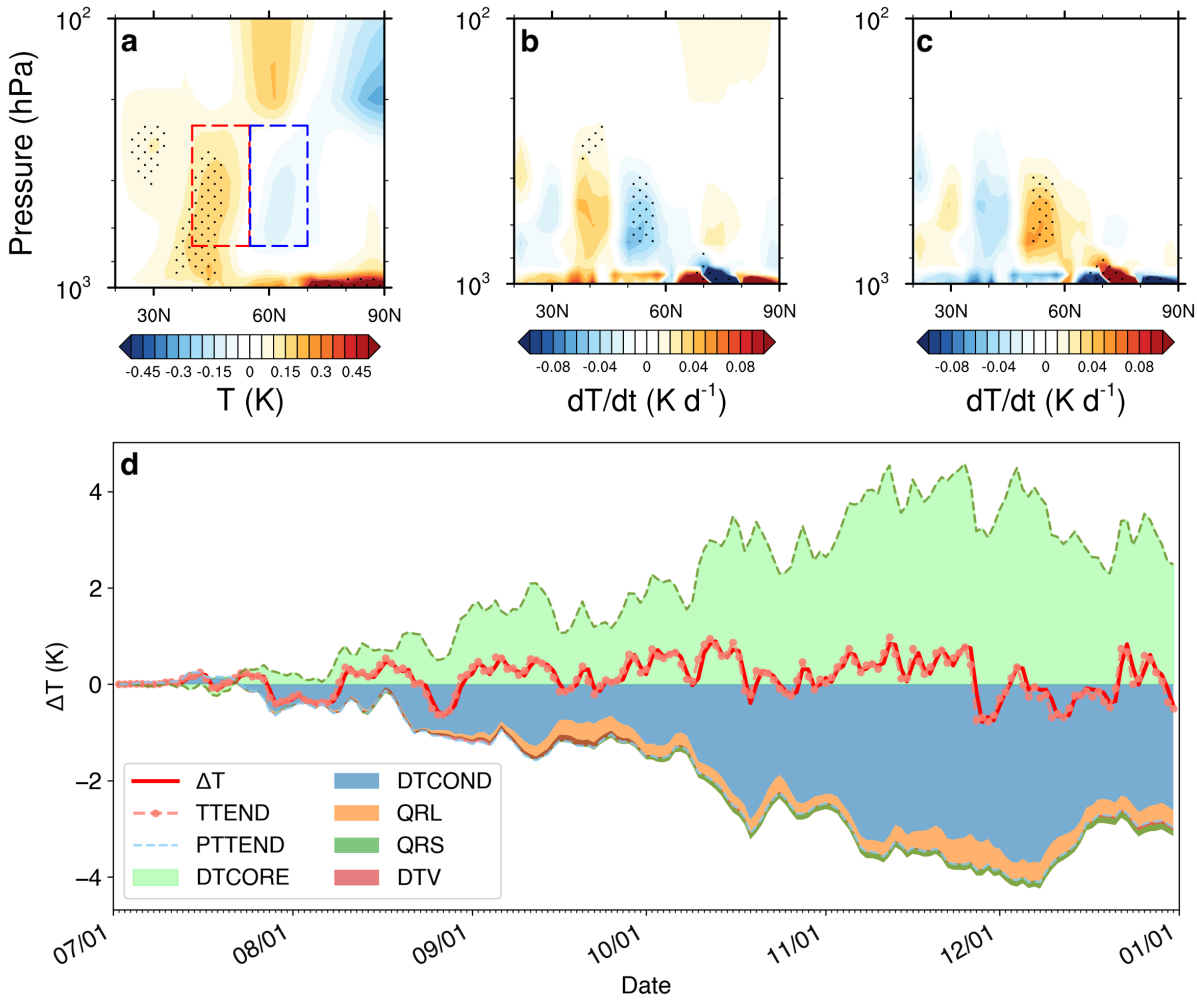


**Supplementary Fig. 7. Air temperature and its tendency responses in the CESM-RESFire experiments. a**, zonally-averaged temperature difference between the SICexp- and SICexp+ sensitivity experiments as shown in Fig. 3c in the main text. The red (blue) box outlines a warm (cool) region in response to the sea-ice perturbation in the SICexp- and SICexp+ experiments, which is averaged for the meridional temperature gradient ($\Delta T = |T_{\mathrm{warm}}| - |T_{\mathrm{cool}}|$) decomposition in **d**. **b**, as in **a**, but for the difference between the SICexp- and SICexp+ experiments in zonally-averaged temperature tendency due to dynamic processes (DTCORE). **c**, as in **a**, but for the temperature tendency difference due to total physical processes (PTTEND). **d**, time series of the meridional gradient in temperature anomaly ($\Delta T$) and its decomposition into

each contributing component, including TTEND as the time integral of the total temperature tendency, PTTEND as the time integral of the temperature tendency due to total physical processes, DTCORE as the time integral of the temperature tendency due to dynamic processes, DTCOND as the time integral of the temperature tendency due to moisture processes, QRL as the time integral of longwave heating rate, QRS as the time integral of shortwave heating rate, and DTV as the time integral of the temperature tendency due to vertical diffusion ($\mathrm{TTEND} = \mathrm{DTCORE} + \mathrm{PTTEND} = \mathrm{DTCORE} + \mathrm{DTCOND} + \mathrm{QRL} + \mathrm{QRS} + \mathrm{DTV}$)). All these terms are calculated as the differences between the SIC- and SIC+ experiments. Stipples in **a-c** show regions that are significantly different from 0 at the 0.1 significance level of a two-sided t-test.

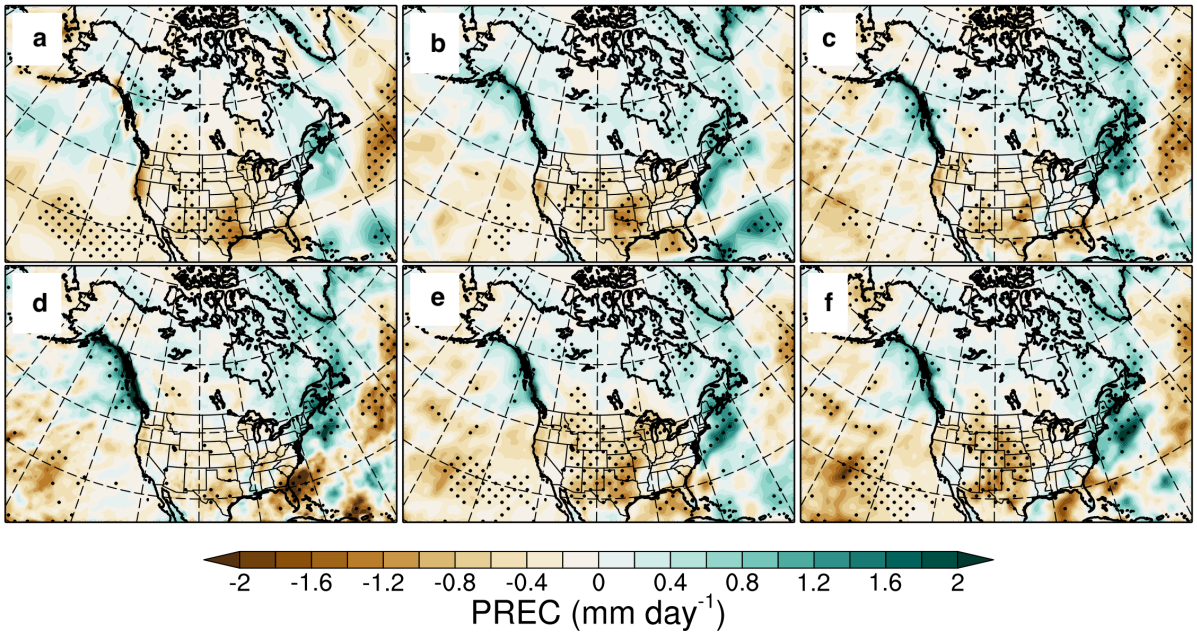


165

166 **Supplementary Fig. 8. The composite difference of the seasonal average (September to**
167 **December) total precipitation rates between the SIC- and SIC+ years based on different**
168 **observational and reanalysis data. a**, the precipitation difference based on the GPCP
169 observational data. **b**, as in **a**, but based on the ERA5 reanalysis data. **c**, as in **a**, but based on the
170 MERRA-2 reanalysis data. **d**, as in **a**, but based on the CFSR reanalysis data. **e**, as in **a**, but based
171 on the ERA-interim reanalysis data. **f**, as in **a**, but based on the JRA-55 reanalysis data. Stipples
172 in **a-f** show regions that are significantly different from 0 at the 0.1 significance level of a two-
173 sided t-test.

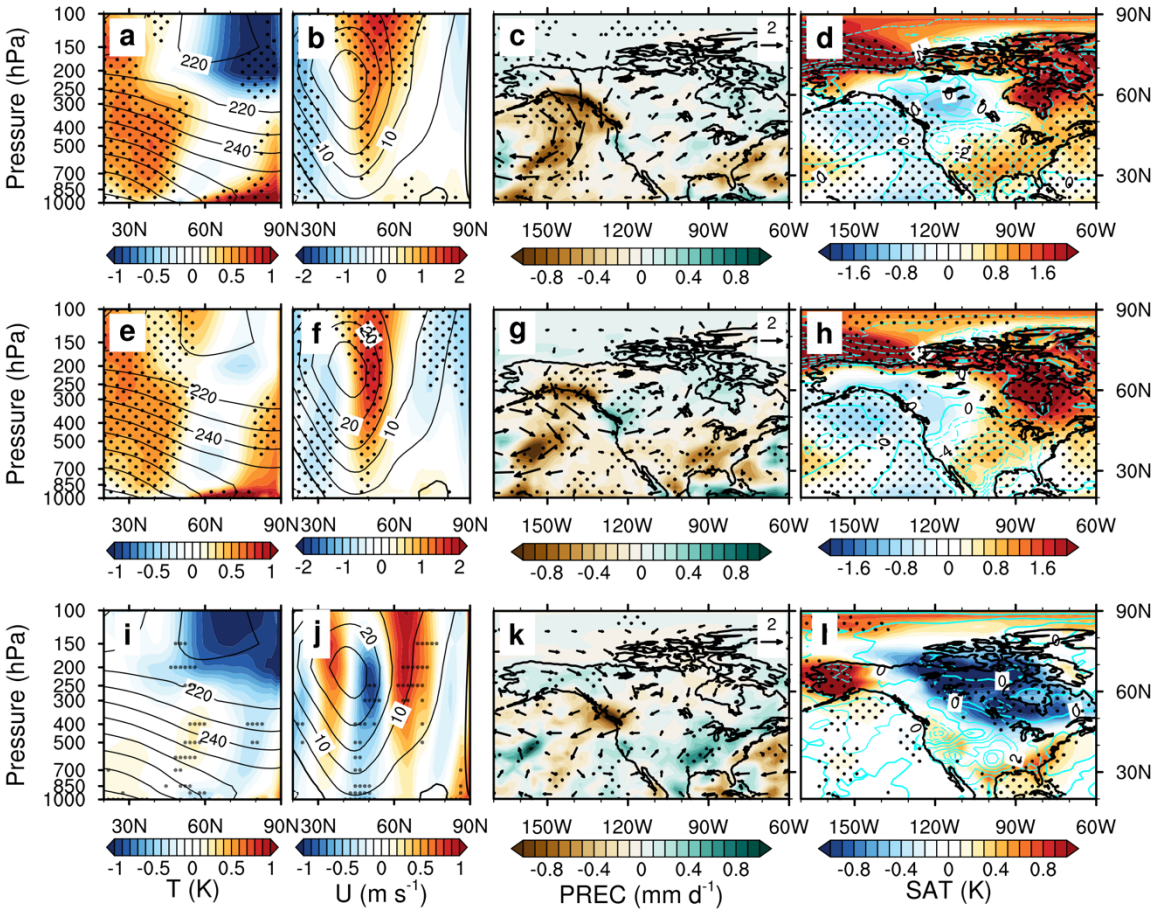


**Supplementary Fig. 9. Climate and fire weather changes between the SIC- and SIC+ years based on the CMIP6 amip and amip-piForcing experiments (4-model ensemble)**. **a**, zonally-averaged (170 °W to 60 °W; as shown in **c**) temperature composite difference (shading) in autumn and early winter (September to December) between the SIC- and SIC+ years (as shown in Fig. 4a) in the amip experiment. The climatology of zonally-averaged temperature in the SIC+ years is also shown (contours; unit: K). **b**, as in **a**, but for zonally-averaged zonal wind in the amip experiment. **c**, as in **b**, but for wind circulation at 500 hPa (arrows; unit: m) and total precipitation rate (shading) differences in the amip experiment. **d**, as in **c**, but for 2-m relative humidity (cyan contours with negative values in dashed lines; unit: %) and 2-m surface temperature (shading) differences in the amip experiment. **e-h**, as in **a-d**, but for the

corresponding variables in the amip-piForcing experiment. **i-l**, as in **a-d**, but for the differences of the corresponding variables between the amip and amip-piForcing experiments. Stipples in **a-l** show regions with all 4 CMIP6 models agreeing on the signs.

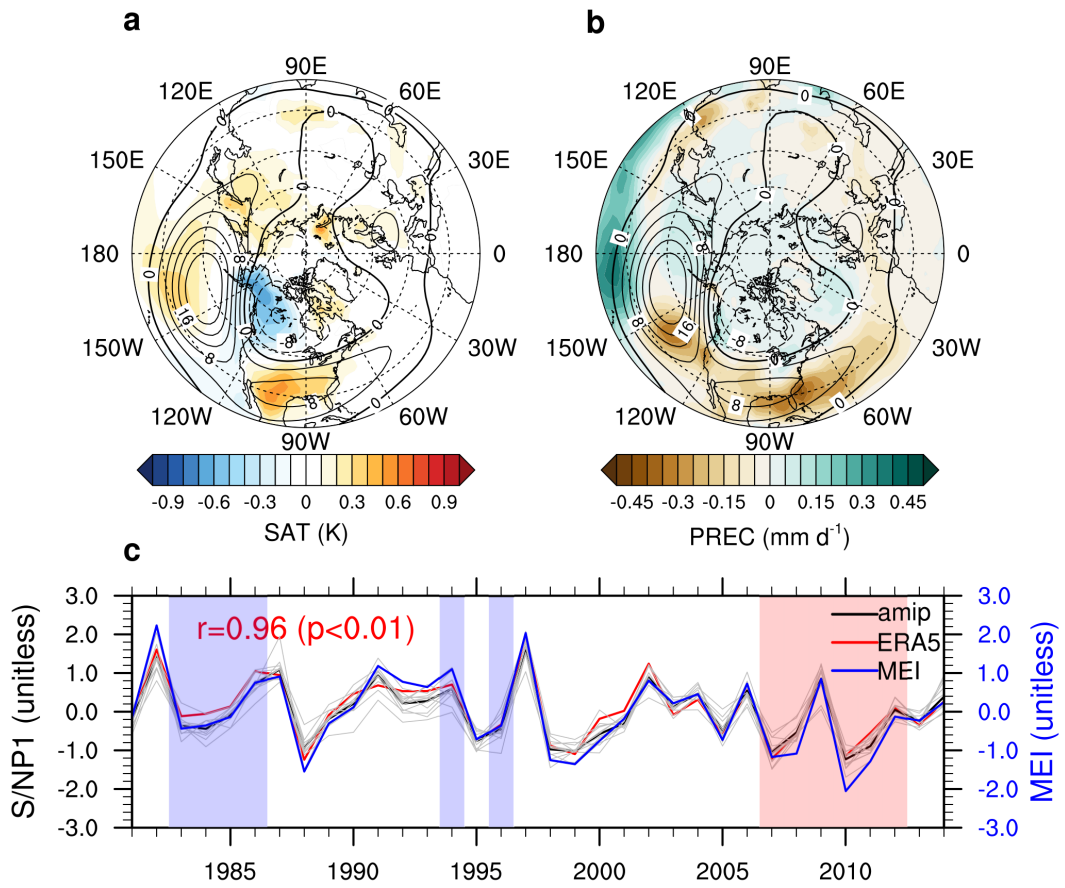


188

189 **Supplementary Fig. 10. The first group of forced responses (S/NP1) in seasonal mean**

190 **multi-field weather variables based on the ERA5 and CMIP6 amip experiment ensemble**. **a**,

191 the composite difference of S/NP1 forced responses in surface air temperature (shading) and

192 Z500 (contours with negative values in dashed lines; unit: m) of the ERA5 data in autumn and

193 early winter between the SIC- and SIC+ years. **b**, as in **a**, but for total precipitation rates

194 (shading) and Z500 (contours with negative values in dashed lines; unit: m). **c**, timeseries of

195 S/NP1 in the multi-variable meteorological fields based on the ERA5 (red thick line) and amip

196 12-model ensemble. The black thick line denotes the 12-model ensemble mean and the grey lines

197 denote results from each model. The MEI (blue thick line) and its correlation coefficient with the

198 ERA5 data (red thick line) are also shown for comparison and interpretation. The vertical bar

199 shading in **c** denotes the SIC- (pink) and SIC+ (blue) years for the composite differences in **a** and

200 **b**.

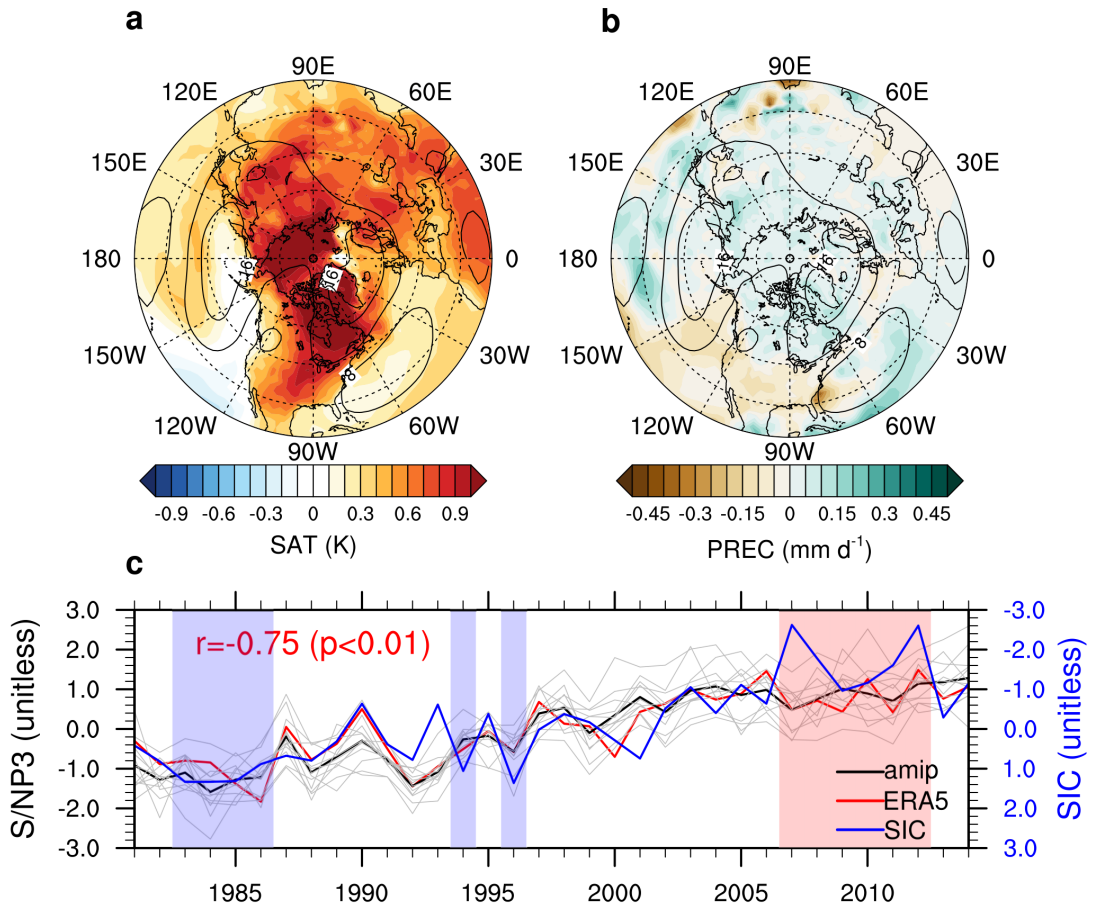


**Supplementary Fig. 11. The third group of forced responses (S/NP3) in seasonal mean multi-field weather variables based on the ERA5 and CMIP6 amip experiment ensemble**. **a**, the composite difference of S/NP3 forced responses in surface air temperature (shading) and Z500 (contours with negative values in dashed lines; unit: m) of the ERA5 data in autumn and early winter between the SIC- and SIC+ years. **b**, as in **a**, but for total precipitation rates (shading) and Z500 (contours with negative values in dashed lines; unit: m). **c**, timeseries of S/NP3 in the multi-variable meteorological fields based on the ERA5 (red thick line) and amip 12-model ensemble. The black thick line denotes the 12-model ensemble mean and the grey lines denote results from each model. The normalized SIC (blue thick line) and its correlation coefficient with the ERA5 result (red thick line) are also shown for comparison and

212 interpretation. The vertical bar shading in **c** denotes the SIC- (pink) and SIC+ (blue) years for the
213 composite differences in **a** and **b**.

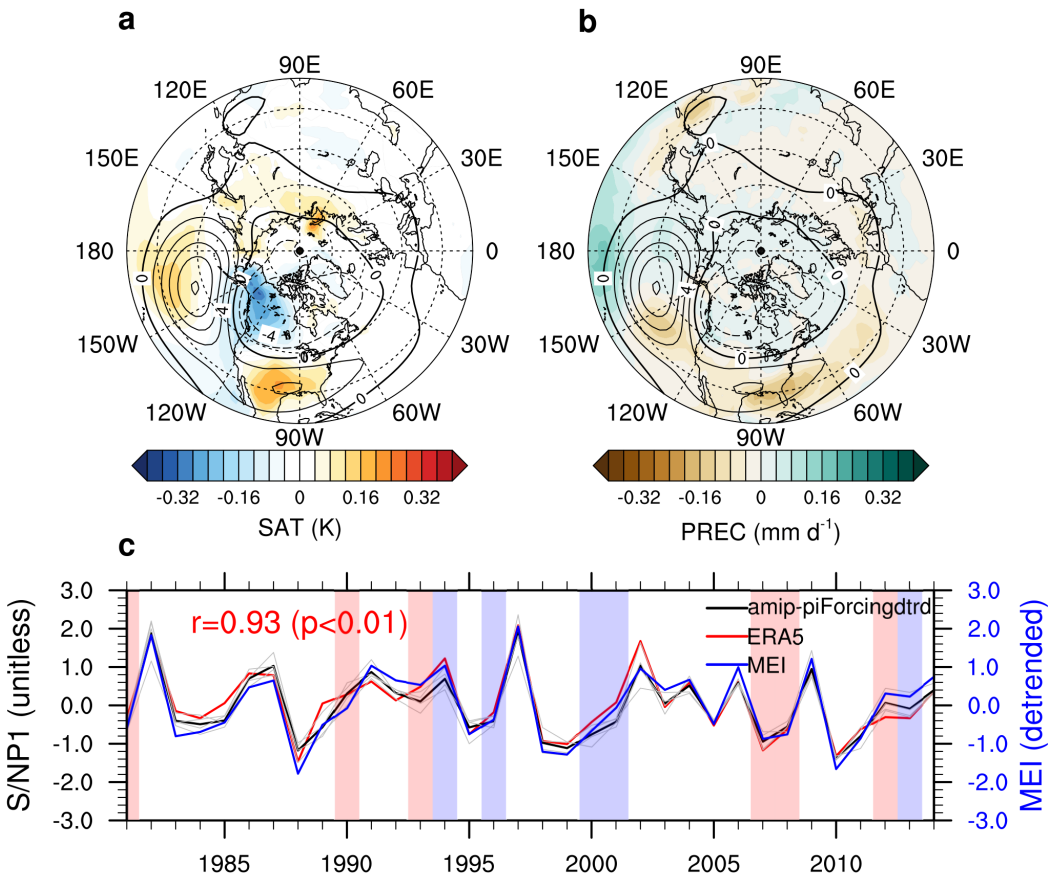


**Supplementary Fig. 12. The first group of forced responses (S/NP1) in seasonal mean multi-field weather variables based on the detrended ERA5 and detrended CMIP6 amip-piForcing experiment ensemble**. **a**, the composite difference of S/NP1 forced responses in detrended surface air temperature (shading) and detrended Z500 (contours with negative values in dashed lines; unit: m) of the detrended ERA5 data in autumn and early winter between the SICnotrd- and SICnotrd+ years. **b**, as in **a**, but for detrended total precipitation rates (shading) and detrended Z500 (contours with negative values in dashed lines; unit: m). **c**, timeseries of S/NP1 in the multi-variable meteorological fields based on the detrended ERA5 (red thick line) and detrended amip-piForcing 4-model ensemble. The black thick line denotes the 4-model ensemble mean and the grey lines denote results from each model. The detrended MEI (blue thick line) and its correlation coefficient with the ERA5 result (red thick line) are also shown for

comparison and interpretation. The vertical bar shading in **c** denotes the SICnotrd- (pink) and SICnotrd+ (blue) years for the composite differences in **a** and **b**.

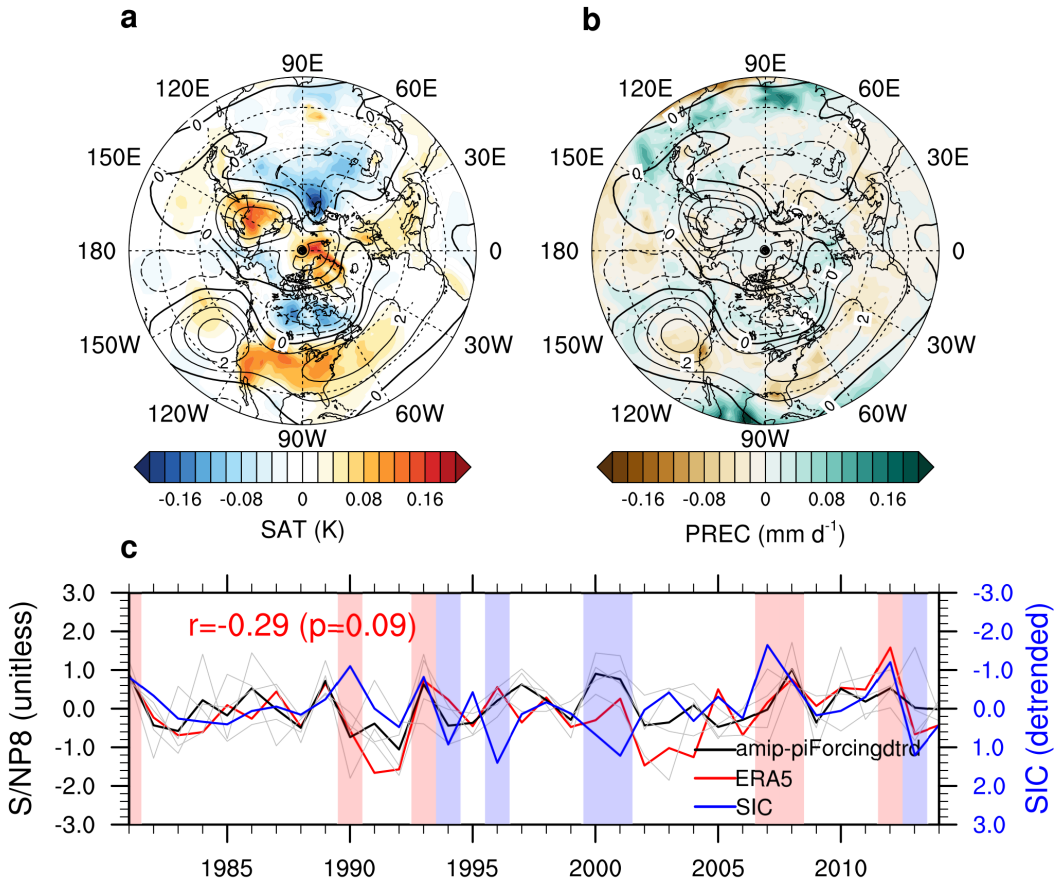


228

229 **Supplementary Fig. 13. The eighth group of forced responses (S/NP8) in seasonal mean**
230 **multi-field weather variables based on the detrended ERA5 and detrended CMIP6 amip-**
231 **piForcing experiment ensemble**. **a**, the composite difference of S/NP8 forced responses in
232 detrended surface air temperature (shading) and detrended Z500 (contours with negative values
233 in dashed lines; unit: m) of the detrended ERA5 data in autumn and early winter between the
234 SICnotrd- and SICnotrd+ years. **b**, as in **a**, but for detrended total precipitation rates (shading)
235 and detrended Z500 (contours with negative values in dashed lines; unit: m). **c**, timeseries of
236 S/NP8 in the multi-variable meteorological fields based on the detrended ERA5 (red thick line)
237 and detrended amip-piForcing 4-model ensemble. The black thick line denotes the 4-model
238 ensemble mean and the grey lines denote results from each model. The detrended SIC (blue thick

line) and its correlation coefficient with the ERA5 result (red thick line) are also shown for comparison and interpretation. The vertical bar shading in **c** denotes the SICnotrd- (pink) and SICnotrd+ (blue) years for the composites differences in **a** and **b**.

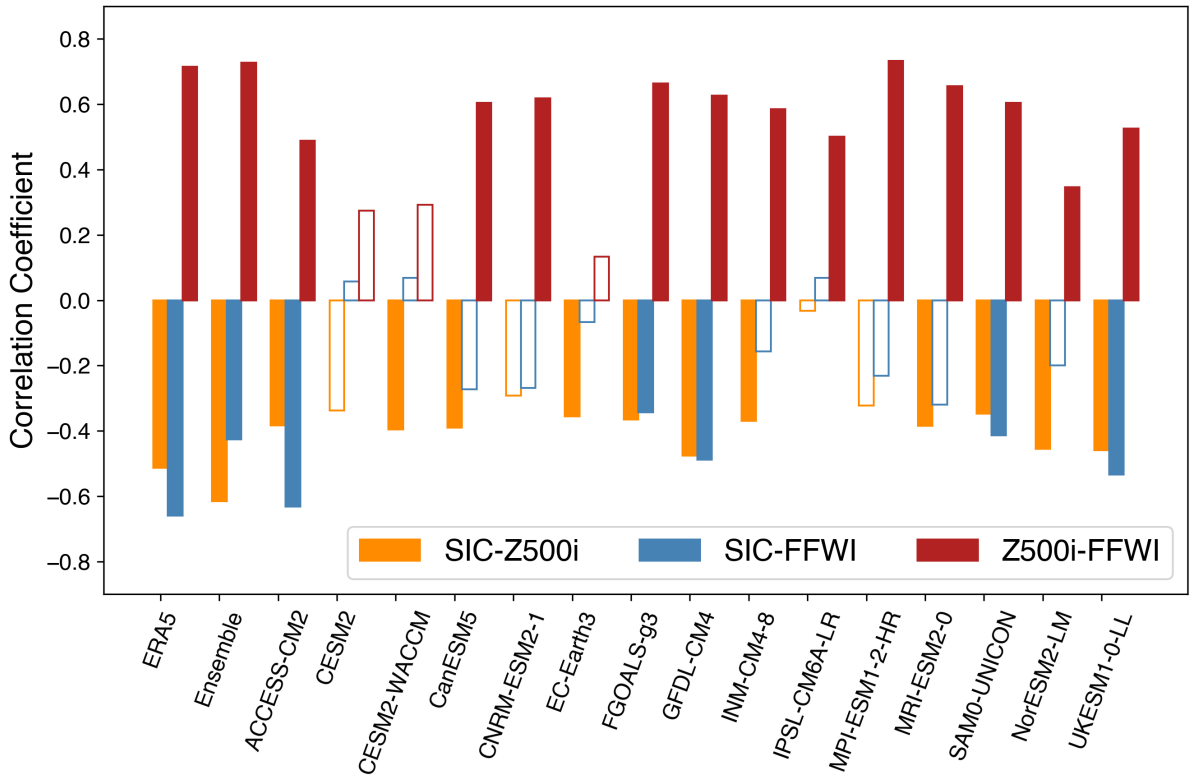


242

243 **Supplementary Fig. 14. Correlation coefficients among SIC, Z500i, and FFWI in the ERA5**

244 **reanalysis data and the amip experiment (1981-2014) based on 15 CMIP6 models and their**

245 **ensemble mean.** The solid-colored bars show correlation coefficients at the 0.05 significance

246 level of a two-sided t-test.

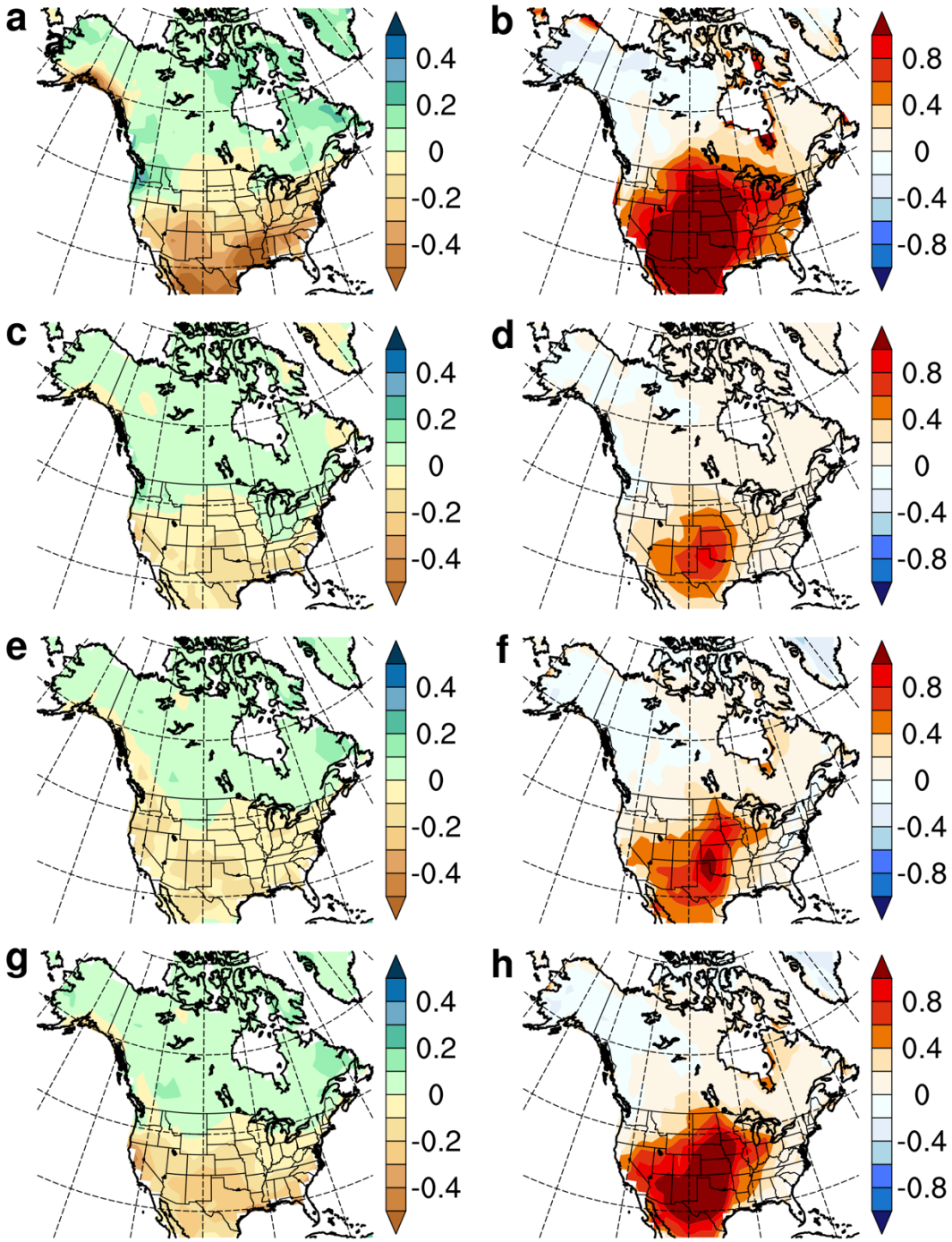


**Supplementary Fig. 15. The composite differences of fire weather variables between the SIC- and SIC+ years**. **a,** total difference in precipitation (unit: mm $d^{-1}$) based on the ERA5 data. **b,** total difference in FFWI (unitless) based on the ERA5 data. **c,** differences in precipitation associated with the ENSO-related S/NP1 pattern based on the S/NP analysis using ERA5 and 12

amip model ensemble. **d,** as in **c** but for differences in FFWI. **e,** differences in precipitation associated with the Arctic-related S/NP3 pattern based on the S/NP analysis using ERA5 and 12 amip model ensemble. **f,** as in **e** but for differences in FFWI. **g,** differences in precipitation as the sum of the ENSO-related S/NP1 pattern and the Arctic-related S/NP3 pattern. **h,** as in **g** but for differences in FFWI.

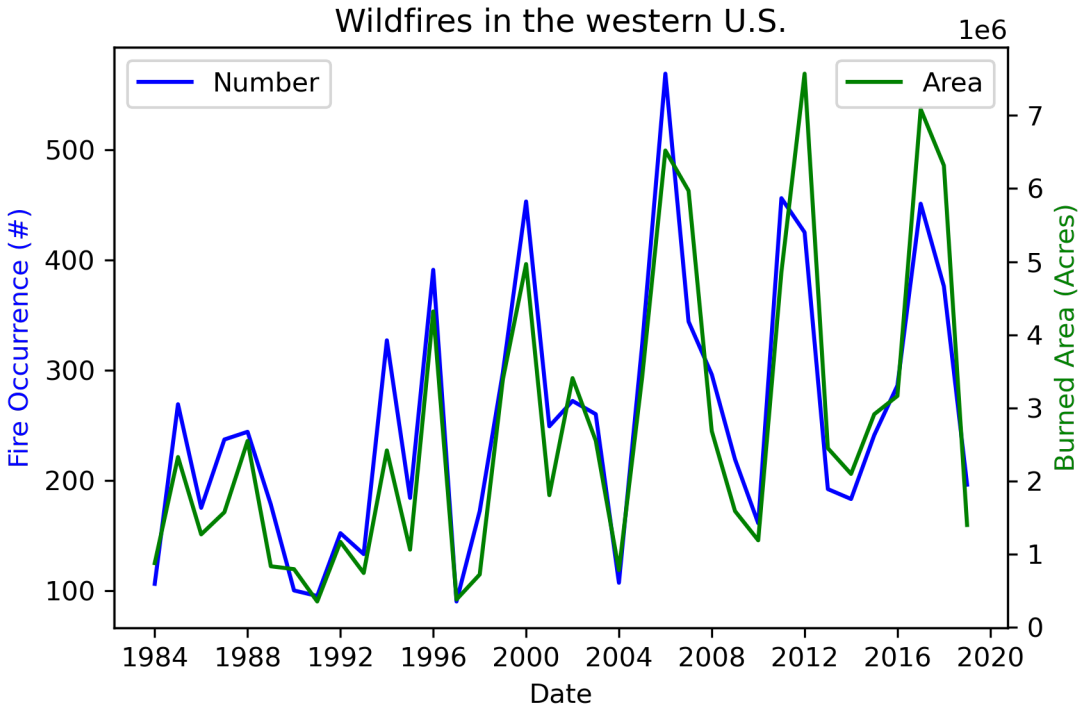


**Supplementary Fig. 16. Updated time series of numbers and total burned areas of large wildfires over the western U.S. based on the latest MTBS dataset[7].**

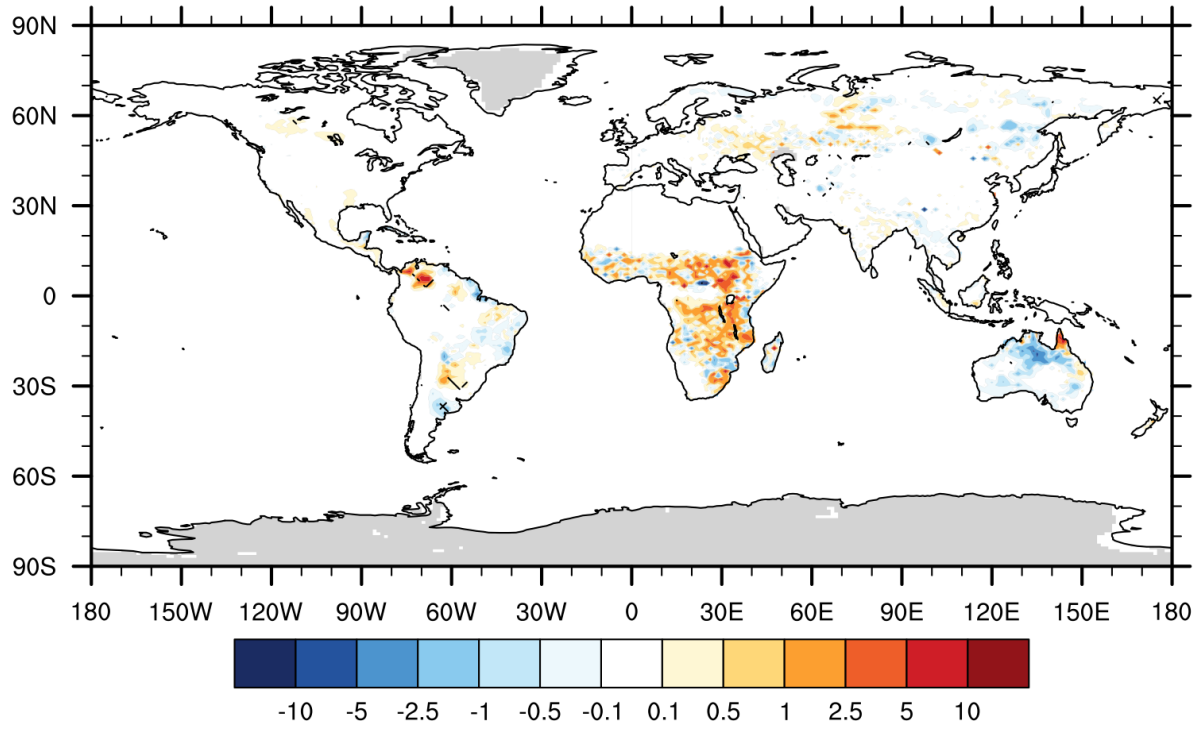


**Supplementary Fig. 17. The net fire feedback effect on global burned area (unit: % $yr^{-1}$) by comparing previous CESM-RESFire sensitivity simulations.** The modeling results are based on the difference between control (CTRL1; with full fire feedbacks) and sensitivity (SENS1B; without fire feedback) experiments adapted from Zou et al.[8].

**Supplementary Table 1. Correlation coefficients between each pair of fire weather indices based on two different reanalysis datasets and their correlations with the SIC time series**

| r (*p*-value) | ERA5-based FFWI | ERA5-based FWI | MERRA-2-based FWI |
|---|---|---|---|
| ERA5-based FFWI | 1.0 | 0.81 (<0.001) | 0.71 (<0.001) |
| ERA5-based FWI | 0.81 (<0.001) | 1.0 | 0.95 (<0.001) |
| MERRA-2-based FWI | 0.71 (<0.001) | 0.95 (<0.001) | 1.0 |
| HadISST-based SIC | -0.68 (<0.001) | -0.58 (<0.001) | -0.37 (0.02) |

**Supplementary Table 2. The modeling settings of the CESM-RESFire sensitivity experiments**

| Experiment | Control | SICexp+ | SICexp- |
|---|---|---|---|
| Time period | 40 years | 40 years | 40 years |
| Horizontal resolution | 1.9°×2.5° | 1.9°×2.5° | 1.9°×2.5° |
| Vertical level | 70 | 70 | 70 |
| Atmosphere | WACCM[(a)] | WACCM | WACCM |
| Land | CLM4.5 with RESFire | CLM4.5 with RESFire | CLM4.5 with RESFire |
| Ocean | Climatology[(b)] | ICE+ year-average regional SST for the Pacific sector of the Arctic[(c)] | ICE- year-average regional SST for the Pacific sector of the Arctic[(c)] |
| Sea ice | Climatology[(b)] | ICE+ year-average regional SIC[(c)] | ICE- year-average regional SIC[(c)] |

[(a)]: using CAM5 physics package and WACCM_MOZART_MAM3 chemistry package;

[(b)]: 1981-2010 average based on the HadISST SST and SIC data[9];

[(c)]: see the main text and Fig. 2a for the region definition;

**Supplementary Table 3. The CMIP6 models in the amip experiment used in this study**

| Model Name | Institute ID | Experiment ID | Ensemble Member |
|---|---|---|---|
| ACCESS-CM2[10] | CSIRO-ARCCSS | amip | r1i1p1f1 |
| CanESM5[11] | CCCma | amip | r1i1p1f1 |
| CESM2[12] | NCAR | amip | r1i1p1f1 |
| CESM2-WACCM[13] | NCAR | amip | r1i1p1f1 |
| CNRM-ESM2-1[14] | CNRM-CERFACS | amip | r1i1p1f2 |
| EC-Earth3[15] | EC-Earth-Consortium | amip | r1i1p1f1 |
| FGOALS-g3[16] | CAS | amip | r1i1p1f1 |
| GFDL-CM4[17] | NOAA-GFDL | amip | r1i1p1f1 |
| INM-CM4-8[18] | INM | amip | r1i1p1f1 |
| IPSL-CM6A-LR[19] | IPSL | amip | r1i1p1f1 |
| MPI-ESM1-2-HR[20] | MPI-M | amip | r1i1p1f1 |
| MRI-ESM2-0[21] | MRI | amip | r1i1p1f1 |
| NorESM2-LM[22] | NCC | amip | r1i1p1f1 |
| SAM0-UNICON[23] | SNU | amip | r1i1p1f1 |
| UKESM1-0-LL[24] | MOHC | amip | r1i1p1f2 |

**Supplementary Table 4. The CMIP6 models in the amip-piForcing experiment used in this study**

| Model Name | Institute ID | Experiment ID | Ensemble Member |
|---|---|---|---|
| CanESM5[25] | CCCma | amip-piForcing | r1i1p2f1 |
| HadGEM3-GC31-LL[26] | MOHC | amip-piForcing | r1i1p1f3 |
| IPSL-CM6A-LR[27] | IPSL | amip-piForcing | r1i1p1f1 |
| MRI-ESM2-0[28] | MRI | amip-piForcing | r1i1p1f1 |

278 **Supplementary Table 5. A list of acronyms used in this study**

| Category | Acronym | Full Name | Description | First Presence |
|---|---|---|---|---|
| Geographic zone | WUI | Wildland-Urban Interface | a transition zone between wilderness and land developed by human activity | Introduction |
| Model type | ESMs | Earth System Models | a coupled modeling system to simulate the interactions of atmosphere, ocean, land, ice, and biosphere and estimate the state of regional and global climate | Introduction |
| Model name | CESM | Community Earth System Model | an Earth system model maintained by the Climate and Global Dynamics Laboratory (CGD) at the National Center for Atmospheric Research (NCAR) | Introduction |
| Model name | RESFire | REgion-Specific ecosystem feedback fire model | a recently developed fire model coupled between the land and atmosphere components of CESM | Introduction |
| Climate variability | AA | Arctic Amplification | the phenomenon that any change in the net radiation balance tends to produce a larger change in temperature near the poles than the planetary average | Introduction |
| Climate index | SIC | Sea Ice Concentration | the area of sea ice relative to the total at a given point in the ocean | First subsection in Results |
| Climate index | FFWI | Fosberg Fire Weather Index | a fire weather index to measure the potential influence of weather on a wildfire based on surface air temperature, wind, and relative humidity | First subsection in Results |

| | | | | |
|---|---|---|---|---|
| Agency name | ECMWF | The European Centre for Medium-Range Weather Forecasts | an intergovernmental organisation supported by 34 States providing operational medium and extended-range forecasts and a state-of-the-art super-computing facility for scientific research | First subsection in Results |
| Climate data | ERA5 | the fifth generation ECMWF atmospheric reanalysis of the global climate | the fifth generation ECMWF atmospheric reanalysis of the global climate covering the period from January 1950 to present | First subsection in Results |
| Composite name | SIC- | minimum SIC years | years with minimum sea-ice concentrations (<-1σ)during the past four decades | First subsection in Results |
| Composite name | SIC+ | maximum SIC years | years with maximum sea-ice concentrations (>1σ) during the past four decades | First subsection in Results |
| Climate variability | ENSO | El Niño-Southern Oscillation | the warm and cool phases of a recurring climate pattern across the tropical Pacific | First subsection in Results |
| Climate index | SST | sea surface temperature | the water temperature close to the ocean's surface | Second subsection in Results |
| Experiment name | SICexp- | CESM-RESFire SIC- experiment | CESM-RESFire sensitivity experiment with perturbed Arctic SIC/SST conditions corresponding to the SIC- years | Second subsection in Results |
| Experiment name | SICexp+ | CESM-RESFire SIC+ experiment | CESM-RESFire sensitivity experiment with perturbed Arctic SIC/SST conditions corresponding to the SIC+ years | Second subsection in Results |
| Climate index | Z500 | Geopotential height field at 500 hPa | a vertical coordinate that approximates the actual height of the 500 hPa pressure surface above mean sea-level | Second subsection in Results |

| | | | | |
|---|---|---|---|---|
| Composite name | SICnotrd- | minimum SIC years after detrending | years with minimum sea-ice concentrations (<-1σ) during the past four decades after detrending | Second subsection in Results |
| Composite name | SICnotrd+ | maximum SIC years after detrending | years with maximum sea-ice concentrations (>1σ) during the past four decades after detrending | Second subsection in Results |
| Climate index | Z500i | Z500 index | Intensity of a fire-favorable circulation pattern in geopotential height field at 500 hPa | Second subsection in Results |
| Climate forcing agent | GHGs | greenhouse gases | gases that absorb and emit radiant energy within the thermal infrared range, causing the greenhouse effect | Third subsection in Results |
| Experiment name | amip | the Atmospheric Model Intercomparison Project | An atmosphere only climate simulation using prescribed sea surface temperature and sea ice concentrations but with other conditions as in the Historical simulation | Fourth subsection in Results |
| Experiment name | amip-piForcing | AMIP SSTs with control forcing | AMIP experiment (with SSTs and Sea Ice the same as in the amip experiment) but with constant pre-industrial forcing levels (anthropogenic & natural) | Fourth subsection in Results |
| Project name | CMIP6 | the Coupled Model Intercomparison Project Phase 6 | a collaborative framework designed to improve knowledge of climate change, being the analog of Atmospheric Model Intercomparison Project for global coupled ocean-atmosphere general circulation models | Fourth subsection in Results |

| | | | | |
|---|---|---|---|---|
| Method name | S/NP | the signal-to-noise-maximizing pattern filtering method | a method to identify spatial patterns (linear combinations of empirical orthogonal functions (EOFs)) with the maximum ratio of signal to noise (with signal defined as variance that is agreed upon across an ensemble) | Fourth subsection in Results |
| Project name | PAMIP | the Polar Amplification Model Intercomparison Project | a coordinated set of numerical model experiments designed to improve our understanding of the Polar amplification phenomenon | Discussion |
| Project name | FireMIP | the Fire Model Intercomparison Project | a coordinated set of numerical model experiments to assess different fire models to establish the reliability of future projects of changes in fire occurrences and characteristics | Discussion |
| Climate data | HadISST | the Hadley Centre Sea Ice and Sea Surface Temperature dataset | a combination of monthly globally complete fields of SST and sea ice concentration for 1871-present | Methods |
| Climate data | MERRA-2 | Modern-Era Retrospective Analysis for Research and Applications, Version 2 | a NASA atmospheric reanalysis that begins in 1980 | Methods |
| Climate index | FWI | Fire Weather Index | a component of the Canadian Forest Fire Weather Index (FWI) system | Methods |
| Climate data | GFWED | the Global Fire Weather Database | a fire weather database that integrates different weather factors influencing the likelihood of a vegetation fire starting and spreading | Methods |

| | | | | |
|---|---|---|---|---|
| Project name | GPCP | the Global Precipitation Climatology Project | Datasets provides monthly, pentad, and daily precipitation analysis from surface and satellite measurements for 1979 onwards | Methods |
| Climate data | CFSR | Climate Forecast System Reanalysis | a third generation global high-resolution reanalysis product coupled atmosphere-ocean-land surface-sea ice system designed to provide the best estimate of the state of these coupled domains over 1979-2017 | Methods |
| Climate data | JRA-55 | the Japanese 55-year Reanalysis | the second Japanese global atmospheric reanalysis project covering 55 years since 1958 | Methods |
| Project name | MTBS | the Monitoring Trends in Burned Severity program | an interagency program whose goal is to consistently map the burn serverity and extent of large fires across all lands of the US from 1984 to present | Methods |
| Climate index | BAC | Fractional burned area change | Fractional changes of the monthly total burned area of large wildfires averaged over the western US between the minimum and maximum SIC years | Methods |
| Model name | CLM4.5 | the Community Land Model version 4.5 | the land model for the Community Earth System Model (CESM) | Methods |
| Model name | WACCM | the Whole Atmosphere Community Climate Model | a comprehensive numerical model spanning the range of altitude from the Earth's surface to the thermosphere in the Community Earth System Model (CESM) | Methods |

| | | | | |
|---|---|---|---|---|
| Experiment name | CTRL | CESM-RESFire control run | the CESM-RESFire control simulation constrained by climatological surface boundary conditions in order to provide intial conditions for the other two sensitivity experiments | Methods |
| Climate index | NFDRS | the National Fire Danger Rating System | a system that allows fire managers to estimate today's or tomorrow's fire danger for a given area | Methods |
| Climate index | BI | burning index | the burning index in NFDRS | Methods |
| Climate index | MEI | the Multivariate El Niño-Southern Oscillation index | the time series of the leading combined Empirical Orthogonal Function (EOF) of five different variables (sea level pressure (SLP), sea surface temperature (SST), zonal and meridional components of the surface wind, and outgoing longwave radiation (OLR)) over the tropical Pacific basin (30°S-30°N and 100°E-70°W) | Methods |
| Method name | EOF | Empirical Orthogonal Function | a multivariate statistical technique partitioning a field into mathematically orthogonal (independent) modes | Methods |
| Model variable | TTEND | total temperature tendency | total temperature tendency | Methods |
| Model variable | DTCORE | T tendency due to dynamical core | temperature tendency driven by dynamic processes | Methods |
| Model variable | PTTEND | T tendency due to total physics | temperature tendency driven by physical processes | Methods |
| Model variable | DTCOND | T tendency due to precipitation physics | temperature tendency driven by moisture processes | Methods |
| Model variable | QRL | Longwave heating rate | temperature tendency driven by longwave heating | Methods |
| Model variable | QRS | Solar heating rate | temperature tendency driven by shortwave heating | Methods |

| | | | | |
|---|---|---|---|---|
| Model variable | DTV | T tendency due to vertical diffusion | temperature tendency driven by vertical diffusion | Methods |
| Model variable | TTGW | T tendency due to gravity wave | temperature tendency driven by gravity wave drag | Methods |

279

**Supplementary References:**


1 Fosberg, M. A. Weather in wildland fire management: the fire weather index, in *Conference on Sierra Nevada Meteorology.* 1-4 (1978).

2 Van Wagner, C. E. Development and Structure of the Canadian Forest Fire Weather Index System. Canadian Forest Service, Ottawa, Canada (1987).

3 Vitolo, C. et al. ERA5-based global meteorological wildfire danger maps. *Sci Data* **7**, 216, https://doi.org/10.1038/s41597-020-0554-z (2020).

4 Field, R. D. *et al.* Development of a Global Fire Weather Database. *Nat Hazard Earth Sys* **15**, 1407-1423 (2015).

5 Copernicus Climate Change Service (C3S). ERA5: Fifth generation of ECMWF atmospheric reanalyses of the global climate . Copernicus Climate Change Service Climate Data Store (CDS). https://cds.climate.copernicus.eu/cdsapp#!/home (2017).

6 Rienecker, M. M. *et al.* MERRA: NASA's Modern-Era Retrospective Analysis for Research and Applications. *J Climate* **24**, 3624-3648 (2011).

7 Eidenshink, J. C., Schwind, B., Brewer, K., Zhu, Z.-L., Quayle, B., and Howard, S. A Project for monitoring trends in burn severity. *Fire Ecology Special Issue* **3**, 19 (2007).

8 Zou, Y. F. *et al.* Using CESM-RESFire to understand climate-fire-ecosystem interactions and the implications for decadal climate variability. *Atmos Chem Phys* **20**, 995-1020 (2020).

9 Rayner, N. A. *et al.* Global analyses of sea surface temperature, sea ice, and night marine air temperature since the late nineteenth century. *J Geophys Res-Atmos* **108** (2003).

10 Dix, M. *et al.* (Earth System Grid Federation, 2019).

11 Swart, N. C. *et al.* (Earth System Grid Federation, 2019).

12 Danabasoglu, G. (Earth System Grid Federation, 2019).

13 Danabasoglu, G. (Earth System Grid Federation, 2019).

14 Seferian, R. (Earth System Grid Federation, 2018).

15 Consortium, E. C.-E. (Earth System Grid Federation, 2019).

16 Li, L. (Earth System Grid Federation, 2019).

17 Guo, H. *et al.* (Earth System Grid Federation, 2018).

18 Volodin, E. *et al.* (Earth System Grid Federation, 2019).

19 Boucher, O., Denvil, S., Caubel, A. & Foujols, M. A. (Earth System Grid Federation, 2018).

20 Jungclaus, J. *et al.* (Earth System Grid Federation, 2019).

21 Yukimoto, S. *et al.* (Earth System Grid Federation, 2019).

22 Seland, Ø. *et al.* (Earth System Grid Federation, 2019).

23 Park, S. & Shin, J. (Earth System Grid Federation, 2019).

24 Tang, Y. *et al.* (Earth System Grid Federation, 2019).

25 Cole, J. N. S. *et al.* (Earth System Grid Federation, 2019).

26 Webb, M. (Earth System Grid Federation, 2019).

27 Boucher, O., Denvil, S., Caubel, A. & Foujols, M. A. (Earth System Grid Federation, 2019).

28 Yukimoto, S. *et al.* (Earth System Grid Federation, 2019).